Design of a single-probe mechanical anemometer for measuring horizontal wind components and direction

R R Mankowski*

(Received in final form October 1991)

Abstract

The work described here sets out the dynamic theory behind the design of a single-probe mechanical anemometer. The probe is the upper extension of a compound pendulum exposed to the wind, wind speed and direction being obtained from the angle of tilt and azimuth angle the pendulum subtends during dynamic equilibrium conditions. A contactless inductor type transducer is used as the positional indicator the output of which varies linearly with wind speed and direction. The uniqueness of the design allows for an extraordinary wide range of sensitivity and working speeds without major mechanical changes. Experimental evidence gained from wind tunnel tests and a field test clearly indicate further improvements are possible and will depend to a large extent on the realization of a reduced scale of the original model.

Nomenclature

A_A	projected area of sensor
C_D	drag coeficient
C_V	viscous damping parameter
D_B	torque arm to centre of buoyant force
D_C	torque arm to centre of mass of shaft assembly
D_D	distance from pivot to centre of sensor
D_R	distance from pivot to centroid of damping vanes
D_W	torque arm to centroid of raised water wedge
d	diameter
f	frequency
f_n, f_d	natural and damped frequency
F_B	buoyant force of submerged damping vanes
F_D	drag force on sensor
F_M	total weight of shaft assembly acting through centroid
F_W	weight of entrained water wedge
g	acceleration of gravity
J	moment of inertia of shaft assembly
K_1, K_2	calibration constants
M	mass of shaft assembly
R_1	oscillation amplitude measured relative to R_2
R_2	distance to new equilibrium position
Re	Reynold's number
T_B	tipping moment resulting from buoyant force
T_C	restoring torque (compound pendulum)
T_D	drag torque acting on cylindrical sensor
T_S	drag torque acting on exposed support shaft
T_W	torque resulting from raised water wedge
V	velocity
V_x, V_y	output voltages for Cartesian (x, y) frame
β	azimuth angle
θ	tilt angle
ρ	density of air
$\dot{\beta}$, $\dot{\theta}$	angular velocities
$\ddot{\beta}$, $\ddot{\theta}$	angular accelerations
ξ	damping ratio

* Associate Professor, Department of Mechanical Engineering, University of Durban-Westville. Private Bag X54001, Durban 4000.

Introduction

Over the period of some sixty years Mechanical engineers involved with anemometry have tenaciously held onto the belief that the basic rotary cup or propeller type anemometer used in conjunction with a vane offers the most rugged and cost effective design for its intended purpose. Not until the last two decades however, have Meteorologists begun to explore the available electronic technology with a view towards increasing sensitivity and response characteristics of wind-sensing instruments. In fact, the trend towards using more sophisticated means of capturing data was the result of demands by Meteorologists to better understand small-scale atmospheric variations such as atmospheric diffusion, boundary-layer development, vortex sensing and eddy correlation measurement near the surface of the earth. Clearly, these demands arose out of public awareness and concern for the detrimental effects associated with air pollution, the greenhouse effect, acid rain, ozone depletion and the movement of radioactive air masses. As a result, a number of innovative designs have been developed and employ techniques such as:

three-component sonic anemometry, Horst [1],
three-dimensional laser doppler anemometry, Prudhommes [2], and
advanced hot-wire anemometry using thermally biased silicon sensors, Van Putten [3]

As anticipated, the frequency response of these sensors is relatively high. The cost of the increased response, in addition to the financial outlay, is the constant attention and maintenance arising from the complex electronics, in-field calibration drift and delicate features. In the majority of electro-mechanical sensing systems it is the question of economics which dictates the level of accuracy employed. As pointed out by MacReady [4], in many cases, the inaccuracy in recording and reading the data causes a far larger error than would be attributed to the sensor itself. In even more cases the variability of the meteorological regime means that the data interpretation warrants only nominal sensor and recording accuracy. Thus for a practical system it is necessary to consider what level of accuracy is really pertinent.

This observation lends some degree of support for the continued use of the conventional cup/propeller and vane anemometer for sustained and relatively maintenance-free measurement. Indeed, these types of anemometers can still be seen decorating the towers and masts of most government installations requiring meteorological information such as the Coast Guard Authority, airports and weather bureaux around the world. It is their very simplicity of design, both mechanically and electronically, which motivates the work about to be described here: the mechanical design of a single probe to measure both wind speed *and* direction. Further impetus for the present work is affoded by a comment made over thirty years ago, McCormick [5],

"Another distressing point is that not all of the instrument makers can tell you what their sensors see and what they do not see, nor how completely or accurately the potential intelligence is displayed in the record, . . . The answer will have to be dug out by means of time-delaying, expensive tests and calibration or, *if one is lucky, by finding some other means to provide the information*". (Italicised emphasis by present author)

General mechanical limitations: cup/propeller and vane anemometers

The mechanical trouble spots associated with these anemometers are relatively few but nevertheless significant enough to merit mention here. Primarily they take the form of frictional effects, aerodynamic inertial effects and nonlinear response characteristics caused by the cross-coupling of second-order effects of the vane (the wind direction sensor) with the first-order effects of the cup or propeller (the wind speed sensor). The literature contains numerous descriptions and analyses of these anemometers, in particular, the design criteria and appraisals based on the general equations of motion: Wieringe [6], Lindley [7], and MacReady [4]. A summary of the most quoted problematic areas are given here in point form.

1. The first and second-order effects impose physical constraints on the distance between the propeller and vane. Gyroscopic coupling effects add further constraints to the inertia of the propeller.
2. As the natural wind often assumes non-horizontal components the cup anemometer will record higher horizontal speeds than the true horizontal mean speed.
3. As a cup wheel assembly accelerates more rapidly with an increase in wind speed than it decelerates in a falling wind, the mean wind recorded is higher than the true mean.
4. For a fixed air flow speed, the vane has a natural and damped frequency which may be excited by one or more of components the frequency spectrum of the passing wind.
5. Due to the inability of the vane to continuously and faithfully align itself with the wind (overshoot and lag phenomena), the propeller cannot always measure the true wind speed. Furthermore, the downwash from the propeller and the gradient of the wind along the vane cause changes in the response characteristics of the vane. The response of the vane in turn depends largely on its damping ratio.
6. Starting torque requires important consideration especially for velocity generating sensors and tachometer/slip-ring assemblies. For a fixed bearing friction, the smaller the cup assembly is, the higher the starting threshold will be. In many applications this narrows the response or sensitivity "window" in which prescribed accuracy specifications are first met.

The above points naturally lead to the general requirements of any electro-mechanical (horizontal component) wind sensor.

1. The wind direction sensor and the wind speed sensor should ideally be uncoupled.
2. The wind speed sensor should be independent of the vertical component of wind.
3. The wind sensor should have a linear response characteristic, ie, have a flat response over the designed wind speed range and be able to indicate the exact mean speed of a sinusoidal wind input.
4. The wind direction sensor should have sufficient damping to reduce the possibility of undesirable resonant conditions being set up. On the other hand, as the damping ratio ξ approaches unity (critically damped system), the response characteristics fall off dramatically.
5. The wind sensor should be sensitive: that is, it should have a quick response to high rates of change in wind speed and direction and therefore a low starting threshold.
6. Lastly, low maintenance and cost of the sensors are critical to their universal acceptance and deployment.

Design features

For clarity in presentation the following discussion is limited to an analysis of a simple mechanical linkage which is equivalent to the dynamic response of the mechanical sensor in the original design presented here.

Referring to Fig. 1, Rigid link A, B, CM, D is pivoted at B where a pair of gimbals allows for a two-degree of freedom system. Thus the spatial configuration of the system is defined by an inclination from the vertical given as θ and a rotation in the horizontal plane β measured relative to a fixed azimuth direction. Hereafter, the link will be referred to as the 'shaft'.

The dynamic pressure sensing probe is a cylinder rigidly attached to the uppermost part of the shaft at A. The dynamic drag force acting on the probe is taken as

$$F_D = C_D \rho V^2 A_A / 2 \quad \text{..... (1)}$$

where F_D is assumed to act at the centroid of the cylinder. For angles of tilt $\theta \leq 10°$ the dynamic drag torque can be approximated to within 2 percent by $T_D = D_D F_D$.

The center of mass (CM) of the shaft assembly is located below the pivot at B and is taken to include the mass of the probe and attached inverted pan. Strictly speaking, the physical configuration of the suspended shaft assembly represents a compound pendulum in that the suspension point is not at the center of mass of the shaft assembly. For planar oscillations, in some fixed azimuth direction (β = constant), and in the absence of any drag

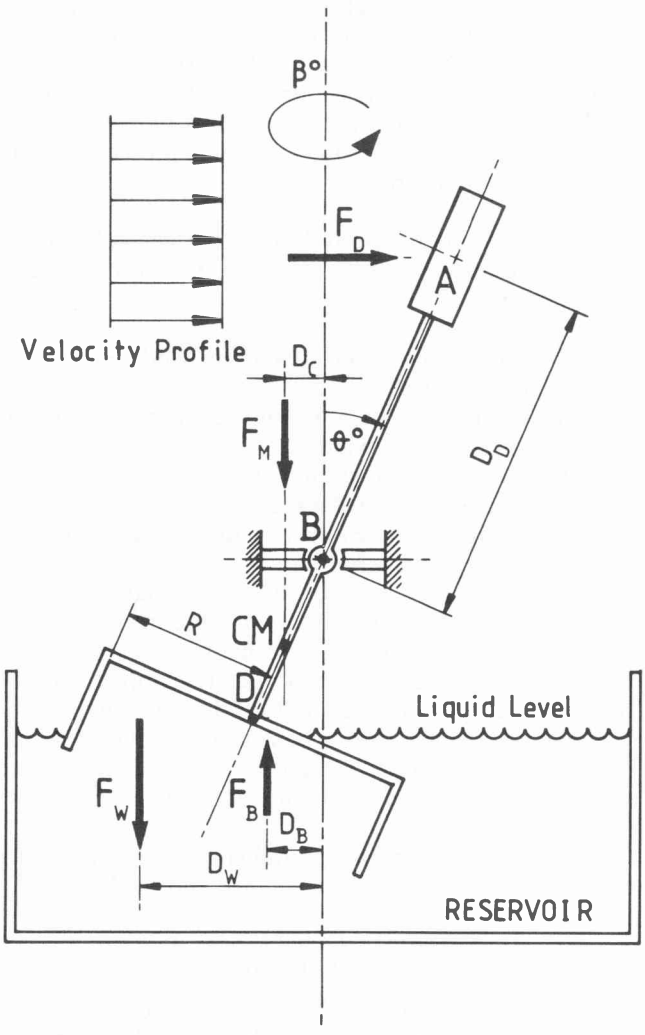

Figure 1 – Two degrees of freedom articulated linkage; highly nonlinear viscously damped (forced) second-order system.

force or damping, the equation of motion for the shaft assembly is given by

$$J\ddot{\theta} + MgD_C = j\ddot{\theta} + F_M D_C = J\ddot{\theta} + T_C = 0 \quad \ldots\ (2)$$

The inverted pan is rigidly attached to the base of the shaft at D and is primarily intended to act as a spatially dependent torque amplifier. As the uppermost portion of the inverted pan is sealed, fluid can only enter and exit from the cavity through the submerged open base of radius R. When the angle of tilt is sufficiently high to cause the inverted pan to break the liquid surface a situation arises in which a negative pressure exists in the fluid entrained in the wedge above the liquid level. This situation is shown in Fig. 1 from which a number of technical points are treated here.

1) The wedge of entrained fluid increases the effective moment of inertia J of the shaft assembly, thus $J = J(\ddot{\theta})$.

2) The weight of the entrained fluid causes a restoring moment T_W about the suspension point B given by

$$T_W = F_W(\theta)D_W(\theta).$$

3) The viscous damping of the shaft assembly is achieved by the submerged cross-vanes centrally located within the inverted pan, Fig. 2. The submerged portion of the inverted pan also contributes to the overall damping. The dynamic damping effect upon the movement of the shaft is thus proportional to the angular velocity $\dot{\theta}$ of the shaft and offers a resisting torque T_R of magnitude.

$$T_R = C_V D_R \dot{\theta}.$$

4) The buoyant force of the submerged pan and damping vanes introduce a tipping moment T_B about the pivot which also must be accounted for. From Fig. 1 this is taken as

$$T_B = F_B(\theta)D_B(\theta).$$

5) A higher-order effect is also introduced into the mechanical behaviour of the system by way of the rising and falling liquid level of the reservoir. As the volume of liquid comprising the wedge increases, the liquid level in the (finite) reservoir lowers itself accordingly and vice-versa. It can be appreciated that the end result of this exchange of potential energy is to further complicate the mathematical form of the moment-arm expressions D_W and F_B as well as the expressions for F_B and J_B.

The influence of this higher-order effect on the mechanics of the system is to 'soften' the tipping moment arising from the buoyant force and to 'harden' the restoring moment caused by the wedge of entrained fluid. Those familiar with nonlinear mechanical vibrations will recognise a parallel to the 'soft' and 'hard' spring characteristics of many nonlinear mechanical vibrating systems.

Equation 2 can now be somewhat refined as

$$J(\theta)\ddot{\theta} + MgD_C(\theta) + F_W(\theta)D_W - F_B(\theta)D_B(\theta) + C_V(\dot{\theta})D_R\theta = F_D D_D \quad \ldots\ (3)$$

Recall Equation 3 has been derived by assuming a constant azimuth angle β. A set of coupled nonlinear differential equations with spatially and time-dependent coefficients would emerge by including the second degree of freedom β into the present analysis. However, in this instance, the desirability of obtaining a closed-form solution for $\theta(t, \beta)$ and $\beta(t,\theta)$, would prove to be a highly complex task if not an intractable one. A much more simplified engineering approach to the problem is presented here by suppressing the acceleration and velocity terms shown in Equation 3. This reduction is tantamount to a static torque-balance analysis of the system. Adopting this approach, Equation 3 is reduced to its final form,

$$T_C + T_W - T_B = T_D \quad \ldots\ (4)$$

where it is understood all the LHS static torque terms are solely functions of θ and of course the geometrical and physical properties of the system. An exact mathematical expression for the wedge torque T_W is given in Appendix 1.

Determination of wind speed and direction

For a constant wind speed and direction ($\dot{\theta} = \ddot{\theta} = \dot{\beta} = \ddot{\beta} = 0$) the shaft assembly will align itself in a manner such that the applied dynamic torque (RHS Equation 4) will be equal and opposite to the sum of the restoring and tipping torques defined by the LHS of this equation. During equilibrium conditions θ can be interpreted directly as a measure of the wind speed. By previous calibration in a wind tunnel it becomes a straightforward exercise to determine the one-to-one correspondence between the actual wind velocity and the angle of tilt, θ. As will be seen later, it is very desirable for this correspondence to be linear. This is so primarily to simplify any electronic signal conditioning prior to data recording or interpretation.

The wind direction (again during equilibrium conditions) is directly proportional to the sweep angle β referenced to an arbitrary zero azimuth angle in the horizontal plane. Put in mechanical terms, the probe will naturally fall down-wind to its final equilibrium position. Irrespective of the wind intensity, β gives a faithful indication of the wind direction and furthermore represents a one-to-one correspondence to all points of the compass.

Without doubt, the most mechanically attractive aspect which can be attributed to the design thus far is the dual nature of the information offered by the 'single' dynamic pressure probe. What remains to be described here is the means by which $\theta(t)$ and $\beta(t)$ can be sensed, recorded and interpreted.

Electronic sensors $\theta(t)$ and $\beta(t)$

The advantages of a contactless inductive-type positional sensor over the conventional tachometer, slip-ring, photo-electric, voltage generating electro-mechanical assemblies are primarily the absence of any mechanical interference/feedback in the form of frictional effects and induced magnetic flux-cutting forces. The inductive sensing unit employed here is an adaptation of a commercially available product such as is found in the joystick unit used in the remote control of model aircraft and X-Y control units found in many of today's computer games. The trade name and specifications of the contactless joystick used in this design are given in Appendix 2 and are solely included for the benefit of the reader and do not imply any form of endorsement of the product.

Fig. 2 illustrates the placement of the major electric components and mechanical mode of operation; for clarity of presentation this is shown with some degree of exaggeration. The general mechanical principles discussed in the previous section are not influenced by the inclusion of this unit since the rigidity of link A, B, CM, D (the shaft in Fig. 1) is still maintained. The application of Equation 3 to the expanded shaft assembly is thus qualitatively and dynamically correct. Provisions for the increased moment of inertia $J(\theta)$, mass M of the shaft and consequent shift of the mass-center are the only quantitative adjustments required to retain the use of the equations given above.

The contactless inductive-type transducer consists of two interactive electro-magnetic coils: the receiving or stationary set is fixed to the same inertial reference frame used for the gimbal support while the transmitting or moving coil is fixed to the principal axis of the shaft assembly. The operating frequency of the inductive circuit is 20 kHz, a frequency far removed from any mechanical resonant conditions of the shaft assembly itself. The null or 'dead spot' of the transducer is constant and occurs when the transmitting coil is centrally located in relation to the nest of receiving or passive coils. The null position is mechanically pre-set when the transmitter coil is aligned in the vertical direction passing through the zenith.

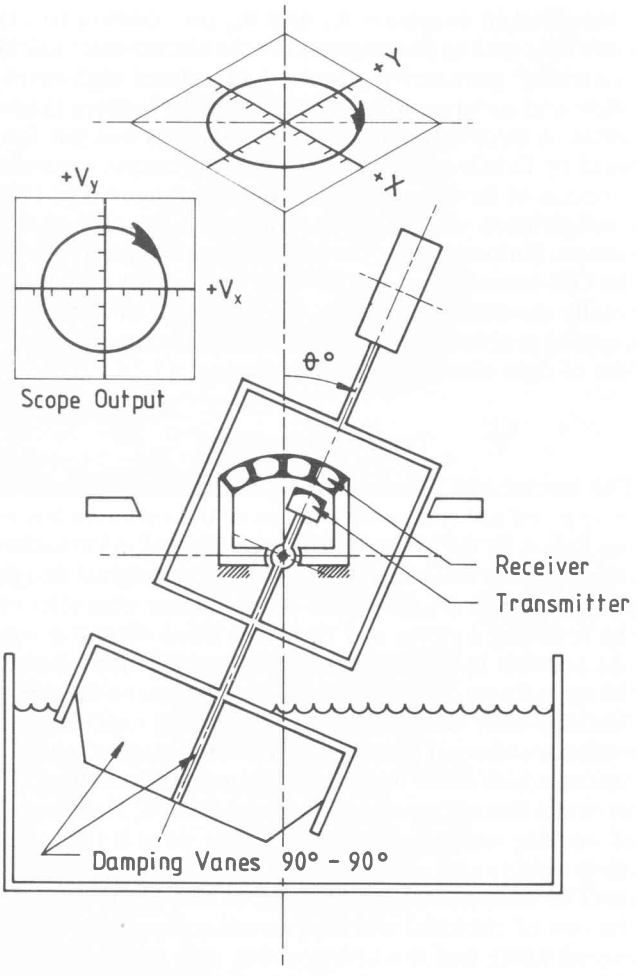

Figure 2 – Operational schematic (not to scale). Note, probe and transmitter are colinear for all angles θ and β.

Two DC output voltages, $V_X(t)$ and $V_Y(t)$, give the vector displacement components of the transmitting coil measured from the null position. As the output voltage of this device is less than one volt, an oscilloscope can conveniently be used to give an instantaneous picture of the shaft alignment. For example, starting at some arbitrary value of β and fixed θ of the shaft and subsequently manipulating the shaft to trace out a circular pattern, a trace similar to that shown in Fig. 2 will be evident. A singular point on the display screen thus corresponds to a unique set of inclinations $(\theta(t), \beta(t))$ describing the orientation of the shaft. The relationship between the voltage output and the inclination set of coordinates is as follows,

$$\theta(t) = K_1\sqrt{V_X(t)^2 + V_Y(t)^2}$$
$$\beta(t) = K_2\arctan(V_Y(t)/V_X(t)) \quad \text{.....} \quad (5)$$

Embedded in constants K_1 and K_2 (in addition to the electronic scaling parameters) are the electro-mechanical 'matching' parameters required to extract high-resolution and accurate information from the sensors themselves. A strikingly similar set of equations was put forward by Drinkrow[8] who analysed the output response function of two propellers mounted orthogonally. This configuration is commonly known as the Gill-anemometer. Unfortunately, the basic mechanical principles of the Gill-anemometer and those of the present design are totally dissimilar. However, his treatment of the 'zero-crossing problem' did offer valuable insight into the problem of data storage and interpretation.

Target specifications

The mechanical nature of the present design is clearly unique and not comparable to any of the anemometers in use today. In the absence of a large body of information regarding the mechanical response of the original design presented here (in particular the nonlinear character of the restoring torques and their combined effects) it was not possible to give explicit target specifications during the early stages of development. For this reason the specifications were determined subsequent to experimental evidence and wind tunnel tests. The only targeted specifications which could be recorded prior to the construction were of a limited general scope and included, 1) the range of working wind speed, 0 to 95 km/hr, (this is the maximum wind tunnel speed which is available in the Department of Mechanical Engineering at this University); 2) the cost of electrical and mechanical components not to exceed R500; and 3) where possible, only standard available components are to be used in the construction of the anemometer.

Further limitations arose in the light of attempting to apply universally accepted response concepts to the present design. Moreover, the uniqueness of the design does not allow the standard testing procedures to be used to establish the response characteristics and specifications of the anemometer as defined by the Meteorological fraternity. These limitations arise from the fact that in general the speed-sensing performance and specifications of mechanical-type anemometers are governed by first-order response characteristics, while the direction-sensing specifications are based on second-order effects. In practice, the wind speed and direction-sensing characteristics are based on a 'distance-constant' and 'delay-distance' respectively. Both characteristics are defined as the length of a column of air passing the particular sensor equal to the product of the wind velocity and the response time taken by the sensor to reach a pre-determined amplitude. The pre-determined amplitude is taken as a fraction of the full excursion amplitude reached after reacting to a step-input or step-change in the wind speed or direction.

For typical cup/propeller speed indicators the distance-constant lies in the range 1.0 m to 7.0 m, Mazzarella[9], and is based on the time taken to reach $(1 - e^{-1})$ or 63 percent of full recovery to the new equilibrium position. For the second-order effects associated with typical mechanical direction sensors such as vanes, the delay-distance lies in the range 0.5 m to 2.5 m and is based on the time taken by the sensor to reach 50 percent of its new equilibrium position.

It is worthwhile to mention here that for 'good' designs both the delay-distance and distance-constant remain invariable over the range of wind speed and wind vector changes for which the anemometers were designed. In the present design, the wind speed *and* direction are determined from a single mechanical probe, the sole response of which is governed by a second-order nonlinear differential equation with time-dependent coefficients. Furthermore, wind tunnel tests clearly show the above mentioned response 'constants' to vary with wind speed. These observations, to a limited extent, justify a qualified use of the delay-distance as a measure of the dual response characteristics of the single probe. The delay-distance as used in this paper will thus be understood to be dependent upon the wind speed.

Range and sensitivity considerations

The drag coefficient D_d for a circular cylinder as a function of Reynold's number is shown in Fig. 3. Assuming standard atmospheric conditions exist over the range of wind velocities $1.0 \text{ m/s} \leq V \leq 26.0 \text{ m/s}$ and fixing the diameter of the cylinder at 20.0 mm, the corresponding Reynold's number lies in the range $1500 \leq Re \leq 3600$. The flow pattern around the cylinder (over this range) is characterised by two types of wake conditions either acting singly or in combination: 1) the so-called Karman vortex trail or vortex street during which downstream eddies break off alternately on either side in a periodic fashion. (The alternate shedding produces periodic forces on the cylinder normal to the undisturbed flow); 2) the flow separates from the cylinder to form a symmetric wake with free shear layers which are turbulent.

It can be shown, Massey[11], that the frequency f with which the vortices are shed from a cylinder is governed by the empirical formula,

$$f = (V/d)\,(0.2 - 3.9/Re)\ \text{Hz}$$

where V is the upstream flow velocity and d the diameter of the cylinder. In terms of the above limits the shedding frequency lies in the range $10.0 \leq f \leq 260$ Hz. Clearly, in the event the damped natural frequency of the shaft assembly lies anywhere in this range, a resonant condition is very likely to be set up. It turns out that the inertial mass $J(\theta)$ of the shaft assembly is sufficiently large to obviate the risk of vortex/shaft excitation. Moreover, it was anticipated that if any undesirable resonant conditions were to occur during testing, sub-harmonic excitation of the shaft via the shedding vortices could well be the cause. Fortunately this was not the case since the damped and undamped natural frequencies of the shaft were respectively 0.25 and 0.70 Hz respectively.

The design range of the windspeed and probe diameter are sufficiently low to insure the critical Reynold's number of 2×10^5 is not reached in practice. For our purposes the working range of Reynold's number will be assumed to be in the range indicated in Fig. 3. Over this range the drag coeficient is relatively constant, $C_d = 1.0 \pm 0.15$ (non-dimensional). Furthermore, the drag coefficient shown here is based on an infinitely long cylinder and

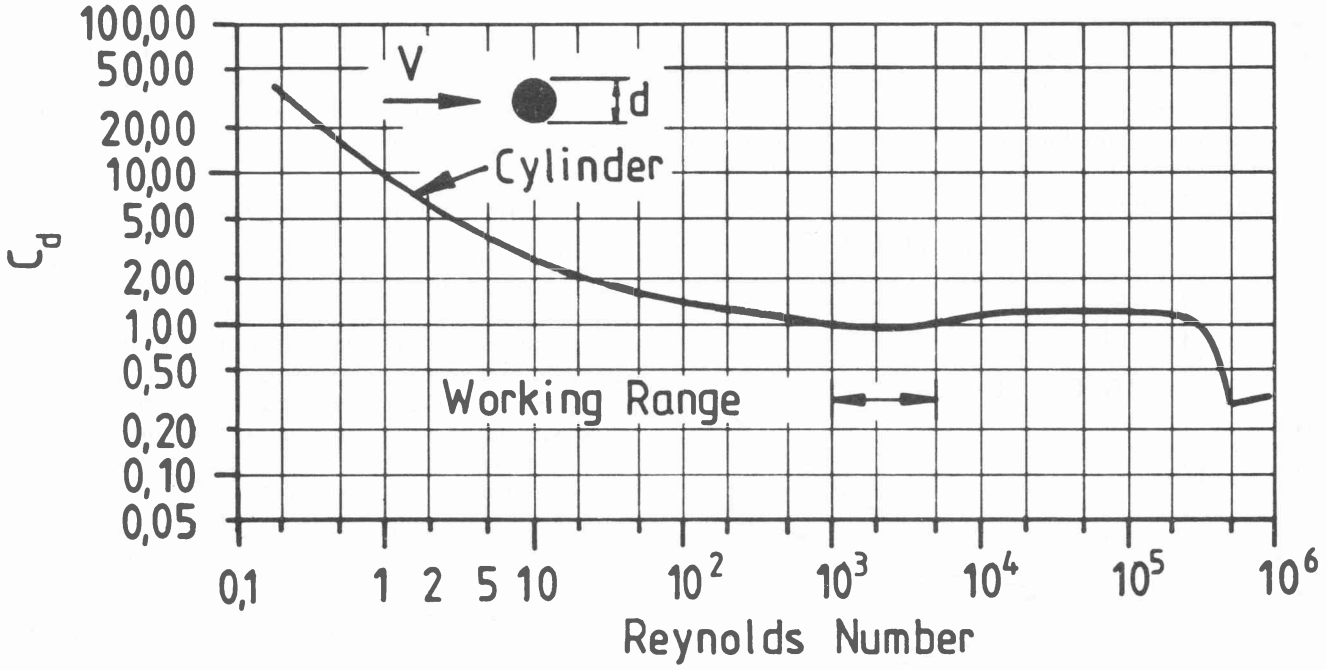

Figure 3 – Drag coefficient for two dimensional flow around cylinder. Area in the drag relation is projected area normal to stream. (Adapted from Binder [10]).

while this introduces errors into the theoretical analysis it is anticipated that wind tunnel tests and subsequent calibration will compensate for the rather complex geometry of the support shaft and finite sensor.

The maximum volume of a right circular cone which can be swept out by the probe arm as a function of (θ, β) is now considered. In particular, the maximum permissible range of θ was required prior to any mechanical design of the shaft assembly being undertaken. Once the relationship between (θ, β) and the output voltage characteristics of the transducer were established in the form of a polar plot, θ_{max} could then be incorporated into the constraints of the design.

A simple calibration test conducted on the original joystick control unit showed that a uniform relationship between (θ, β) and the output voltage exists for $\theta \leq 9.5°$ and is of the form

output voltage (vector) = transducer gain × sin (4.77θ) ..... (6)

'Uniformity' used here indicates that for all values of β, a predetermined value of θ (for a fixed transducer gain) could be measured to within 2 percent accuracy using the polar relationship set out by Equations 5 and 6. As a matter of interest, the manufacturers of the joystick control unit set 18° as the mechanical limit to the tilt angle. The measured error in the polar uniformity of this outer range however was an unacceptable 15 percent.

The mechanical sensitivity of the anemometer is primarily controlled by the offset distance at which the center of mass of the compound pendulum is located from the pivot point. The shorter this distance is, the higher will be the sensitivity (other parameters assumed constant). It can be appreciated that any desired sensitivity within practical reason is possible and for the most part depends on the choice of maximum design wind speed for full scale deflection ,$\theta_{max} = 9.5°$.

As mentioned earlier, a linear relationship between the wind speed and the output voltage is sought, ie, wind speed = K_3 (output voltage) where K_3 is the electronic gain control of the transducer network. As the drag force on the sensing probe varies as the square of the velocity, the overall design requires a mechanical means whereby the total restoring torques are directly proportional to the wind speed. This was accomplished in two phases: firstly, by physically 'tuning' the mechanical system in the wind tunnel. This included identifying and quantifying the coupled-effects of varying the torque arm lengths, projected area, density and viscosity of fluid, and the action lines of the nonlinear restoring forces offered by the inverted pan and wedge of entrained fluid. Secondly, it remained to optimise a set of mechanical parameters (with the aid of a digital computer) in order to establish a practical configuration which would produce a linear and accurate relationship between wind speed and output voltage. A storage oscilloscope used in conjunction with the wind tunnel speed indicator were indispensable in this exercise.

Calibration

The governing equation for static equilibrium conditions, Equation 4, was translated to a digital computer. In the computer analysis the RHS of this equation was transferred to the LHS with the result that an analytic solution could be obtained by solving for an implicit form of an equation using iterative methods. The vector sum of both tipping and restoring torques is represented by the dashed line along the abscissa axis, Fig. 4. The computer program used to generate the torque-balance produced here, incorporated the relationship between θ and the trans-

ducer output voltage, Equation 6. Attention is drawn to the independence of θ and wind speed on the 'zero' solution to the torque-balance. The final set of physical parameters chosen and implemented in the design are defined by the individual torque terms appearing in Fig. 4. All of the relevant physical data form the contents of Table 1, Appendix 3.

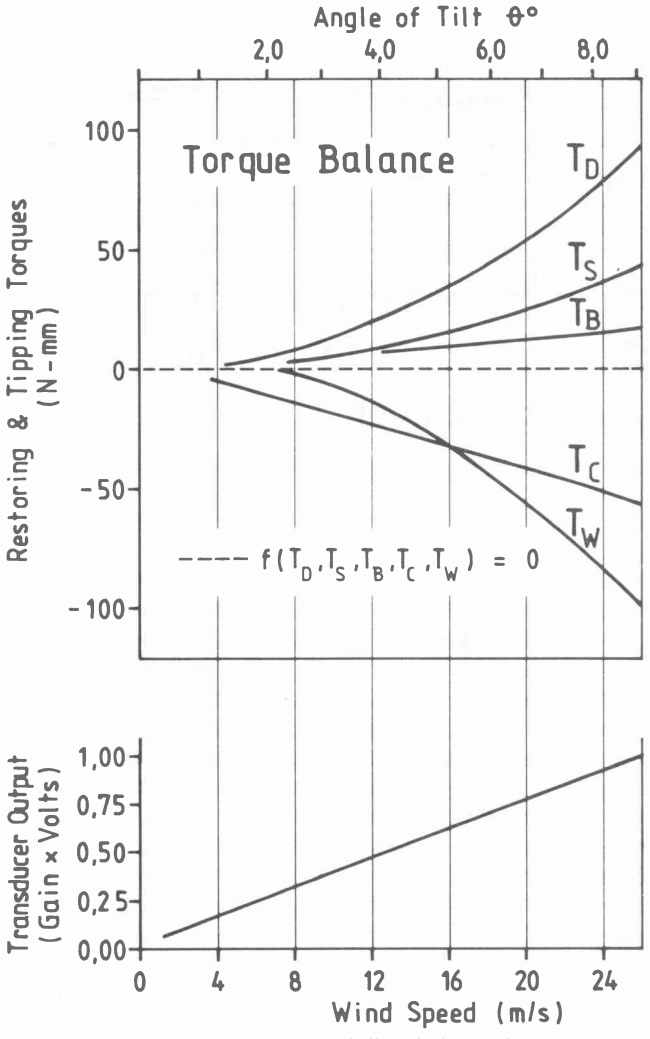

Figure 4 – Relation among angle of tilt, wind speed, torques and transducer output.

Referring to Fig. 4, the theoretical analysis shows the second-degree characteristic of the torque balance exercise. A theoretical accuracy of 2 percent over this working range is based on the full-scale deflection of 100 N-mm along the ordinate axis. Of particular interest is the trace described by T_W, the restoring torque offered by the wedge of entrained fluid. T_W is first seen to appear around 2° while the remaining torques all start at the origin. This 'late' appearance is a result of a 3 mm thick layer of fluid flooding the upper-outer surface of the inverted pan. By varying this thickness the effect of T_W could be delayed and made to take effect anywhere up to the full angle of tilt $\theta_{max} = 9.5°$. As the wedge torque has the steepest of the restoring torque gradients, the final choice of ratios amongst the radius of the pan, flood depth, and pivotal distance was the most critical in exacting an accurate solution to the torque-balance.

The results of an experimental investigation, also shown in Fig. 4, established the linear relationship to persist in all four quadrants, $0 \leq \beta \leq 360°$. This was verified by rotating the anemometer in various wind flow settings and evaluating the wind velocity vector.

Appraisal: wind tunnel experiments

Owing to the fact that the speed measured by cup/propeller sensors is governed by a first-order effect and that the speed sensing probe in the present design is governed by a second-order effect, there is little justification to provide a comprehensive comparison or cross-reference between these two different 'ordered' systems based on accepted specifications. A similar complication is introduced when consideration is given to the second-order direction sensing components of this and other designs. It becomes a highly complex task to isolate the speed from the direction response characteristics arising from a single mechanical probe. For these reasons the majority of the performance characteristics are presented without reference to data available in the literature. It is hoped that the performance data presented here in discussion and graphical form contain sufficient information for Meteorologists and reseachers to judge the accuracy and sensitivity in the light of their experience and insight.

Two delay-distance characteristics were investigated: 1) for a fixed wind tunnel speed the probe was released from its zenith position and allowed to 'fall' to its new equilibrium position, and 2) from a fixed angle of tilt θ (representative of a known wind speed) the probe was released and allowed to 'rise' to its natural zenith equilibrium position. This latter method did not require the use of the wind tunnel.

The first method determined the anemometer's response to a step input and was a measure of the acceleration characteristic. The second method also investigated the response to a step input but in this case was a measure of the deceleration characteristic. The step input here was tantamount to a sudden 'shut-off' of the wind speed.

By comparing the acceleration and deceleration delay-distance characteristics it is possible to give a qualitative assessment of the averaging ability of the anemometer during continuously varying wind conditions. Recall that the cup anemometer accelerates faster than it decelerates when reacting to a sinusoidal wind speed input and therefore records a higher 'true' mean wind speed. Errors in the range of 7 to 12 percent higher than the true mean speed have been recorded in the literature, Lindley[7].

Fig. 5 gives an indication of the differences between the delay-distances calculated from the acceleration and deceleration wind tunnel tests described above. Also included here are the response times taken by the probe to reach 50 percent of the new equilibrium positions. The fact that the acceleration periods are consistently larger than the deceleration periods suggests that the anemometer would indicate a lower than true mean wind speed when placed in a sinusoidally varying wind environment. It is noted that this under-run error is more pronounced for the higher speeds and is therefore attributed to the retarding viscous forces which are proportional to velocity. An approximation to the percent error expected in the higher range is unfortunately not possible at this junc-

ture. Of interest is the local change of concavity for all four curves at around 11.0 m/s and is for the most part attributed to the nonlinear viscous effects and inertial damping forces reflected in the dynamic equation of motion, Equation 3. The percent over-run associated with cup/propeller anemometers are usually determined experimentally in wind tunnels equipped with 'gust generators' to produce a controlled sinusoidally pulsating flow of variable speed, amplitude and frequency.

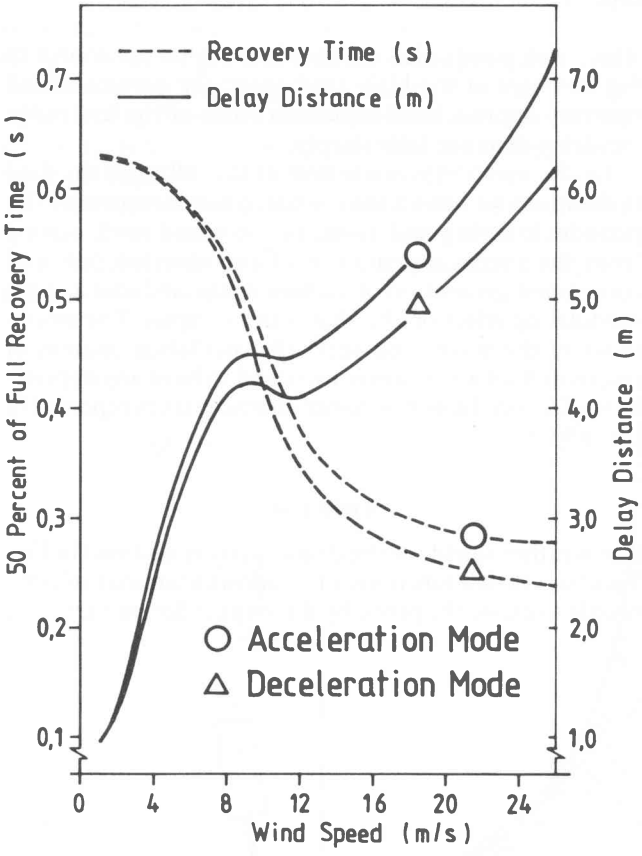

Figure 5 – Experimental data: best-fit curves generated from over 25 points for each trace (Power paraffin as reservoir fluid).

Initially, it was thought that a relatively high viscous fluid would minimise the occurrence of excessive overshoot and forced mechanical vibration of the shaft assembly. A common light motor oil was used for this purpose in the early stages of the wind tunnel experiments. The subsequent response characteristics however were very poor compared to the delay and distance constants of the majority of commercially available cup/propeller/vane anemometers in use today. The major reason for the poor performance was the apparent 'slowness' with which the oil clinging to the outside surface of the inverted pan slid down the inclined disc on its return to the reservoir. An improvement of 200 to 300 percent in the delay-distance was evident when the motor oil was replaced with power paraffin. Fig. 6 gives an account of the percent overshoot taken from the acceleration and deceleration tests described above. The percent overshoot is calculated as a ratio R_1/R_2 where R_1 is the maximum excursion amplitude measured relative to the new equilibrium position and R_2 the distance between the original offset and the new equilibrium position. As 'overshoot' is intimately related to the concept of damping ratio, a discussion of these to response characteristics is presented below.

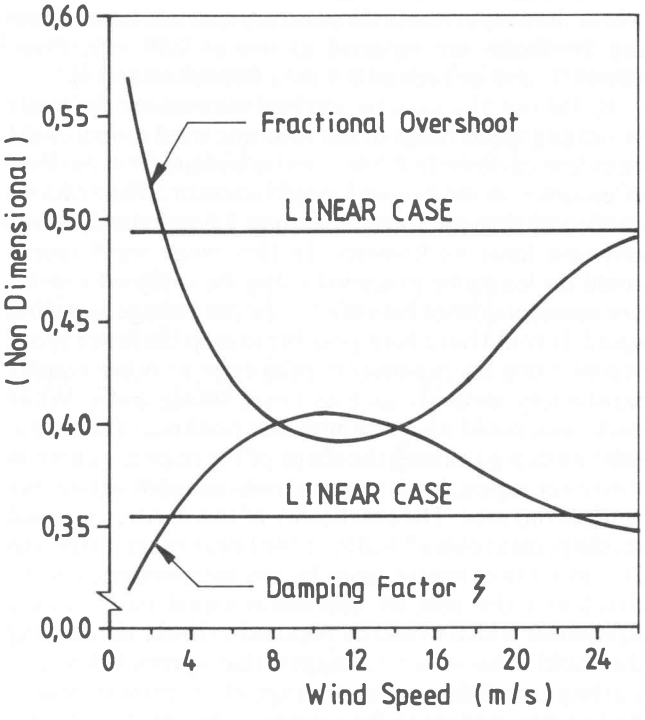

Figure 6 – Dependence of damping ratio and percent overshoot on wind speed. Calculated from storage oscilloscope traces.

It is beyond the intended scope of the present paper to examine the precise response characteristics resulting from different fluid densities and viscosities. Rather it was decided to use one which simply produces the desired effect within accepted accuracy limits and minimal cost. One qualitative observation however is worthy of mention here; in the event the anemometer is to be used in a low-variation wind environment where the delay-distance is of secondary importance, a motor oil would be well suited for this purpose because the mean wind speed in this instance is obtained from a mechanical averaging of the wind fluctuations taken over a time span of 30 to 60 seconds. Furthermore, this inherent mechanical averaging ability does not require the use of costly and complex signal processing equipment to extract the mean wind speed.

In respect of time averaging techniques, most meteorological demands are met by an estimation of the mean wind speed from observations that are of less duration than the required averaging time. In favourable contrast, Hardy[12] found that a 3 to 5 minute averaging time was a optimal sensing duration to minimise errors in estimation. With the advent of microprocessors these estimates are obtained by exponentially-mapped-past and slope averaging techniques.

The choice of viscosity can thus be interpreted as a means of controlling a pre-selected time window over which averaging and accuracy are optimal. Obviously, higher viscous fluids will have the effect of increasing the sample time. A trade-off point or compromise between the percent overshoot and delay-distance must be identified and will depend on the needs of the user, the ex-

tremes of the meteorological regimes and required accuracy being the primary considerations.

The definition of starting threshold is the lowest speed where the output meets the accuracy specifications. Starting thresholds are reported as low as 0.09 m/s, Fritschen[13], and as high as 0.9 m/s, SethuRaman[14].

By the use of a variable inclined manometer the lower indicating speed range of the subsonic wind tunnel could be extended down to 0.5 m/s and maintain the same level of accuracy as the original speed indicator. Observations confirmed that for speeds less than 1.0 m/s the dynamic response loses its linearity. In this range wind speeds could no longer be predicted using the designed one-to-one correspondence between the output voltage and wind speed. It could have been possible to map the lower speed regime using an exploratory pilot tube or other equally satisfactory methods such as timed smoke puffs. While such tests could also establish the nonlinear functional relationship governing the shape of the response curve in this lower region, basic practical reasons inhibited further work in this area. The practicality of this decision is based on the present overall width of the linear range 1.0 m/s to 26.0 m/s, (an extensive range by any meteorological standard) and the cost of additional signal conditioning equipment which would be required to lower the starting threshold. This is not to suggest that speeds below this starting threshold are out of range of the present design. By suitable changes to the moment arms, probe area and geometry of the inverted pan it would be possible to alter the working range to say 0.1 m/s to 2.6 m/s over 9.5° of full tilt angle θ_{max}. Of course, the lower limit to any desired starting threshold will depend on the starting torque which, in turn, is dependent upon the bearing friction of the gimbal support.

Another 'constant' measure of the response characteristics found in anemometer specifications is the damping ratio ζ where $0.0 \leq \zeta \leq 1.0$. The results of an experimental investigation, Monna[15], into the dynamic properties of three different commercially available propeller vanes show that the damping ratio 'usually' lies in the range 0.4 to 0.7. It is a measure of the amount of damping in a linear second-order system and for relatively low values of ζ the system will oscillate for a long period of time before coming to rest while for values of ζ approaching unity (critical damping) the system will monotonically approach a new equilibrium position with zero percent overshoot. Mathematically ζ, R_1, and R_2 are related by

$$\zeta^2 = 2\ln(r)/(2\ln(r) - \pi^2), \; r = R_1/R_2.$$

The ratio r is commonly used to determine the log-decrement of a damped vibrating system, Prentis[16], and is well suited to the study of vane response. When the natural and damped unforced frequencies f_n and f_d are known, ζ can also be calculated by $\zeta = f_d/f_n$. The damped and undamped natural frequencies of the shaft assembly were obtained respectively by timing small planar oscillations with and without fluid in the main reservoir. Assuming f_d and f_n are constant over the range of θ and wind speed, $\zeta = f_d/f_n = 0.248/0.699 = 0.355$. This damping ratio and its related fractional overshoot are shown in Fig. 6 as linear cases. In the actual wind tunnel tests a different set of response curves emerged and are shown here to be wind speed dependent. Two points immediately stand out:

1) at wind speeds around 11.0 m/s the shaft response is relatively highly damped with minimal overshoot at this speed,

2) for the extreme low and high ranges of wind speed the anemometer's response is clearly more sensitive to the time-rate-of-change of the wind velocity vector.

These two points also substantiate the trends shown in Fig. 5 where at the high wind speed the percent of full recovery approaches a minimum while at the low range the delay-distance falls steeply.

Lastly, mention is made here of the influence the fluid in the reservoir has on the overall dynamic response. The periodic lowering and rising of the liquid level, arising from the oscillatory motion of the inverted pan and consequent generation of surface waves, induces a slight modulating effect on the shaft output signal. The amplitudes of the waves and vertically oscillating column of reservoir fluid are however too small to have any appreciable effect on the performance characteristics reported in this paper.

Field test

The weather shield for the drum cavity is outlined in Fig. 7 and serves two functions: (1) it allows a laminar velocity profile to excite the probe by directing reflected turbulent

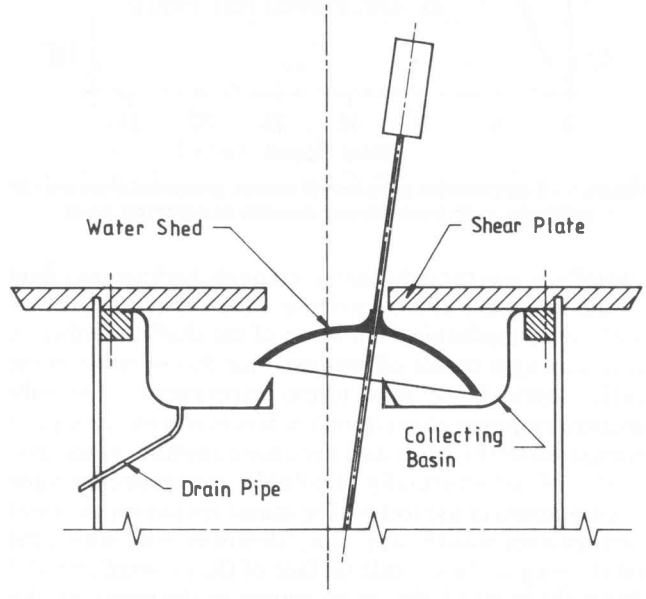

Figure 7 – Fundamental operation of weather shield (not to scale).

air flow downwards and around the side of the drum and (2) any rain entering the center hole of the shear late is channeled to a drain tube by way of the annular collecting basin. As the liquid level and density of the reservoir fluid is critical to the sensitivity of the anemometer this feature is essential for prolonged field operation.

The anemometer was mounted on top of a 2 metre re-

search control room. The room itself is located on the roof of the Faculty of Engineering complex and is relatively free from eddy interference such as down wash from adjacent buildings. During a three week installation period extending from mid January 1991 the anemometer was intermittently exposed to the extremes of Natal summer conditions. Aside from the occasional topping-up of the liquid level because of fluid being lost by evaporation and the return trips to the laboratory for 'final' mechanical adjustments and zero settings, very little maintenance was required.

The transcribed recording shown in the upper two traces of Fig. 8a was achieved first by capturing the data on a Nicolet 310 digital storage oscilloscope and then transferring it to a datalogger computer for printing on an x-y plotter. The sampling rate was set at 20 points per seconds. The 140 s record typifies the wind behaviour during the morning hours of that day: a steady 1.0 m/s to 2.0 m/s east-north-east wind with modulating gusts up to 15.0 m/s. The magnitude and direction of the wind vector are shown in Fig. 8b and Fig. 8c respectively and were calculated using Equation 5 in conjunction with the calibration curve of Fig. 4. A source of comparison is given by the dashed horizontal line appearing in Fig. 8b and represents the official 'average' wind speed of 3.3 m/s obtained from the Office of Environmental Affairs Durban Branch for February 12 1991 at 09h00. The official wind direction was given simply as 'north-east'. The difference between the official and experimental data here is partly attributed to the wind-channeling effects of the adjacent Umgeni Valley and surrounding hills of the University.

At the time of preparing the final draft of this manuscript the weather conditions in Durban were unfortunately well-behaved and did not present a challenging variety of wind flow patterns for monitoring. The very limited data reported here does however contain sufficient detail to be able to extrapolate or predict the general response characteristics which could be expected over the higher average wind speeds.

Of immediate interest is the modulating damped natural frequency (period 4.0 s) impressed on the dotted locus of points, Fig. 8a. The dotted trace will be referred to here as the 'carrier' speed and is intended to indicate a rough approximation to a signal which would occur without the modulating effects. As the absolute velocity and azimuth angle are derived directly from the carrier speed, the effects of the damped natural frequency are not shown on these graphs.

It can be expected that if the frequency spectrum of a variable wind contains periodic components near 4.0 s and is travelling at low speeds, the correlation of data in this case would be very poor. Monitoring conditions would be further exacerbated by steep wave fronts which give rise to large overshoot and subsequent oscillations. The low damping ratio at low wind speeds is the major cause for this behaviour. Since the damping ratio is also low for the extreme high speed range of the anemometer, a similar modulating effect is envisaged to occur there. The best response and correlation are therefore expected to occur at mid-range (10.0 m/s to 15.0 m/s) where the damping ratio and percent overshoot are relatively favourable, Fig. 6.

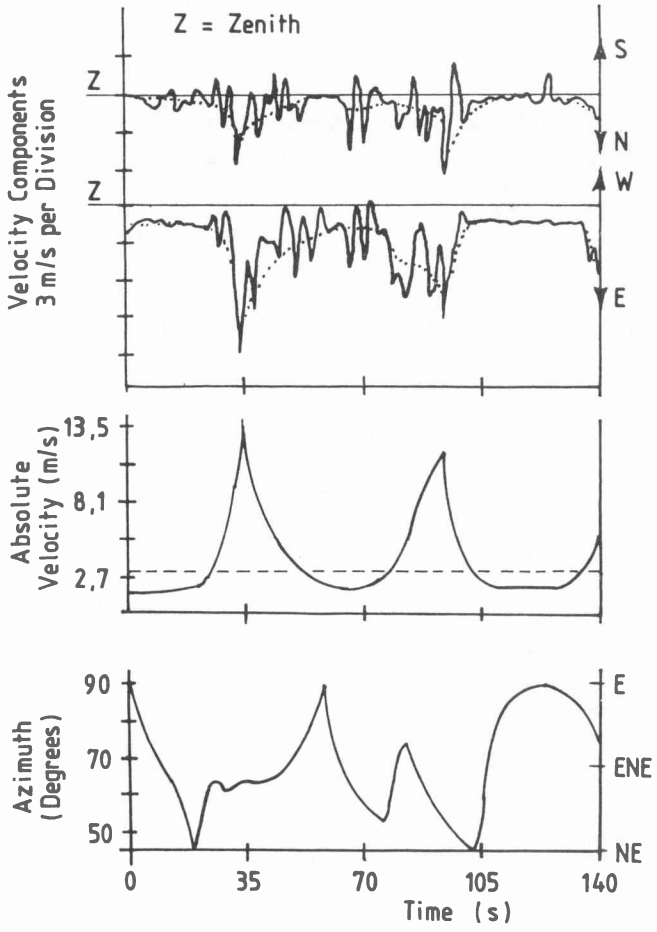

Figure 8 – Field test data and reduced information.

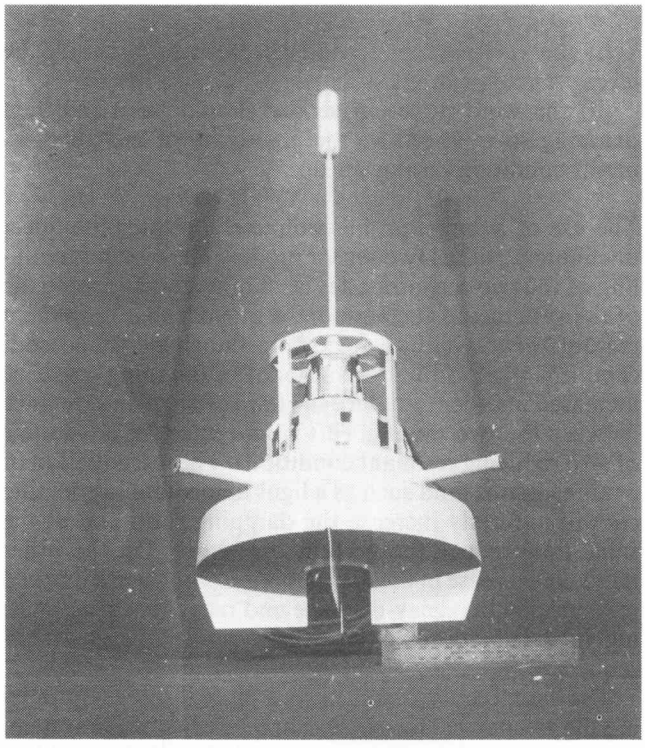

Figure 9 – Shaft assembly mounted on retaining ring. Ring is fixed to inner drum surface by three cantilevered bolts, 120° – 120° – 120° (Patent Pending).

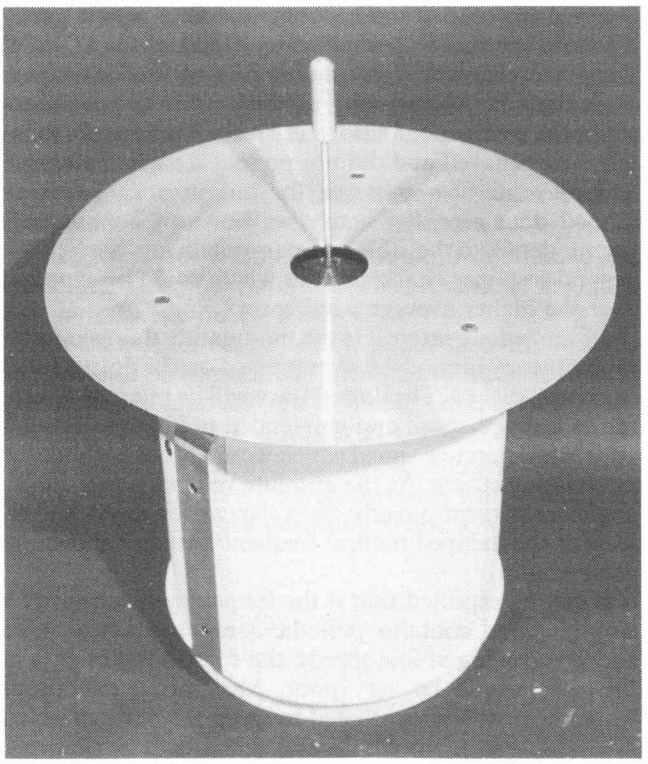

Figure 10 – Assembled single probe anemometer. Side channel fixed to reservoir houses drain pipe and filler plug.

Summary and recommendations

The field test demonstrates the design to fall short of the targeted features and requirements set out in the early sections of this work. Of the requirements mentioned, two have not been met and are repeated here as,

(i) the direction and wind speed sensors should be ideally uncoupled, and
(ii) the wind direction sensor should have sufficient damping so as to reduce the possibility of unstable resonant conditions being set up.

The use of a single probe completely negates the 'ideal uncoupling'; of the two sensor modes. The dynamic coupling of the two sensor modes is an inherent characteristic of the system and furthermore is one of the more salient features of the design. Accepting the single-probe concept, it is thought that the amount of damping could be increased in order to reduce the level of cross-interference between the two modes. This would have the advantage of also reducing resonant conditions. The introduction of a more viscous fluid such as a light to medium lubricating oil will naturally increase the damping ratio and at the same time reduce the percent overshoot. On the other hand, an increase in the damping ratio will have a marked influence on the delay-distance and response-time resulting in a reduction of the overall sensitivity as a consequence.

The damping ratio thus plays a pivotal role in optimising the mechanical response characteristics of the system. At this stage of development, it is believed the problem can best be approached by further experimental work directed at smoothing out the modulating 'noise' levels mechanically. Such efforts could well identify and quantify the optimal range of fluid densities and viscosities for a given set of weather conditions. Once this is accomplished, the decision of using (expensive) electronic signal conditioning equipment can be weighed against the required accuracy and the resultant accuracy of the improved model.

Regarding the choice of fluid, volatility must also be borne in mind. Liquid paraffin (Appendix 3) for example, compared to power paraffin is in general a more suitable fluid; it is less volatile and has a higher density and viscosity. The vapour pressure and chemical composition of liquid paraffin are also potentially less harmful to the solid state electronic board and mechanical bearings located directly above the fluid level line within the 'sealed' reservoir.

The construction of a scaled-down version of the present model is very possible and desirable. The benefits of such scaling, in addition to reducing the bulk and space requirements, lie in the fact that the natural frequency varies inversely as the square root of the fundamental dimensions of the shaft assembly. Thus for a reduced scale of 1/4 the natural frequency is doubled. This is particularly attractive since the dynamic compliance of the shaft assembly is subsequently increased with a proportional decrease in the delay-distance characteristic. To what extent a scaled-down version will react to fluids of similar viscosity, and the consequential reduction of damping area, is unkown. Until a thorough dimensional analysis is undertaken and a reduced scale model constructed, this question will remain tantalizing.

Acknowledgement

A vote of thanks is recorded here to Professor R M Morris, Dean of the Faculty of Engineering at this University and to Professor L Roberts, Dean of the Faculty of Engineering at the University of Natal for their contagious enthusiasm and support for this work. To Mr B Marcus for his high technical standards maintained in the workshop, I am deeply indebted. Lastly, I take this opportunity to thank Dr G L Bishop for his sustained interest in seeing this design through to its conclusion.

References

1. Horst, T. W. Spectral transfer functions for a three-component sonic anemometer. J. Appl. Metero. Vol. 12, No. 6. Sept. 1973. pp. 1072-1075.
2. Prudhommes, S., and Serudie, A. Design of a three-dimensional doppler anemometer for T2 transonic wind tunnel. ICIASF Conference paper. Sept. 1989. Published by IEEE, Piscataway, NJ, USA. pp. 197-205.
3. Van Putten, A. F. Advanced silicon anemometer design with constant voltage-to-current ratio biasing. E. I. Conference presented at EUROSENSORS: Fourth symposium on sensors and actuators, Part 2. May, 1989. pp. 615-621.
4. MacReady, P. B., and Jex, H. R. Response characteristics and Meteorological utilization of propeller and vane wind sensors. J. Appl. Meteor., Vol. 3, April, 1964. pp. 183-193.
5. MacCormick, R. A. Wind and turbulence instrumentation for air pollution studies. 175th Nat'l Mtg., Amer. Meteor. Soc., March, 1959.
6. Weiringa, J. Evaluation and design of wind vanes. J. Appl. Meteor., Vol. 6, Des. 1967. pp. 1115-1122.
7. Lindley, D. The design and performance of a 6-cup anemometer. J. Appl. Meteor., Vol. 14, Sept. 1975. pp. 1135-1145.
8. Drinkrow, R. A solution to the paired Gill-anemometer response function. J. Appl. Meteor., Vol. 11, Feb. 1972. pp. 76-80.
9. Mazzarella, D. A. An inventory of specifications for wind measuring instruments. Bull. Amer. Meteor. Soc., Vol. 53. No. 9, Sept. 1972. pp. 861-871.
10. Binder, R. C. Fluid Mechanics. Prentice-Hall, New Jersey USA., 1962. pp. 170.

11. Massey, B. S. Mechanical Fluids. D. Van Nostrand, London. 1968. pp. 288-289.
12. Hardy, R. N. A note on the optimum averaging time of wind reports for aviation. Meteor. Mag., Vol. 103, 1974. pp. 99-105.
13. Fritschen, L. J. A sensitive cup-type anemometer. J. Appl. Meteor., Vol. 6, Aug. 1967. pp. 695-699.
14. SethuRaman, S. and Brown, R. M. A comparison of turbulence measurement made by a hot-film probe, a bivane, and a directional vane in the atmospheric surface layers. J. Appl. Meteor., Vol. 15, Feb. 1976. pp. 138-144.
15. Monna, W. A. A. Experimental data on the dynamic properties of several propeller vanes. J. Appl. Meteor., Vol. 18, May 1979. pp. 699-702.
16. Prentis, J. M. Dynamics of mechanical systems. London, Longman. 1970. pp. 277-282.

Appendix 1

d = depth of fluid above submerged pan for $\theta = 0$
L = BD (m)
R = Radius of Pan (m)
Wedge Torque begins only when pan breaks liquid surface, or for $\sin(\theta) > \dfrac{d}{L\tan(\theta) + r}$

Assign:

$$M = L\tan\left(\frac{\theta}{2}\right) - \frac{d}{\sin(\theta)}$$

$$P = -\frac{M}{R}$$

$$I_1 = \frac{R^4\pi}{16} - \frac{\sin^{-1}(P)R^4}{8} - \frac{M(R^2-M^2)^{\frac{1}{2}}(R^2-2M^2)}{8}$$

$$I_2 = \frac{M(R^2 - M^2)^{\frac{3}{2}}}{3}$$

$$I_3 = \frac{(R^2 - M^2)^{\frac{3}{2}}}{3}$$

$$I_4 = M\left(\frac{\pi R^2}{4} + \frac{M(R^2 - M^2)^{\frac{1}{2}}}{2} - \frac{R^2\sin^{-1}(P)}{2}\right)$$

$$XBAR = \left(\frac{I_1 + I_2}{I_3 + I_4}\right)$$

$$ZBAR = \frac{\tan(\theta)(I_1 + 2I_2 + MI_4)}{2(I_3 + I_4)}$$

$$WW = \text{Wedge Weight} = 2\tan(\theta)(I_3 + I_4)(S.G.\ 9810) \quad (N)$$

$$\text{Torque} = WW[\sin(\theta)(L + ZBAR) + XBAR\cos(\theta)]10^3 \quad (\text{n-mm})$$

Appendix 2

Contactless joystick stock no. 162-984
The RS contactless joystick employs an inductive sensing system and is recommended for application where the operational life time is the limiting factor. The joystick is designed to give an output voltage swing directly comparable with 270° potentiometers in a 55° joystick, i.e. giving a voltage swing equivalent to + and −10% of the supply voltage.

The sensing system operates at impedances of only a few hundred Ohms and is therefore not sensitive to moisture. The electronics are sprayed with protecting varnish. The copper windings are totally potted, and only brass and stainless steel are used elsewhere.

The screening can is black anodised aluminium, and the main body glass filled Nylon. The gaiter is Neoprene, and the retaining bezel Acetal. The knob is Bakelite, retained by a chemically blacked tolerance ring.

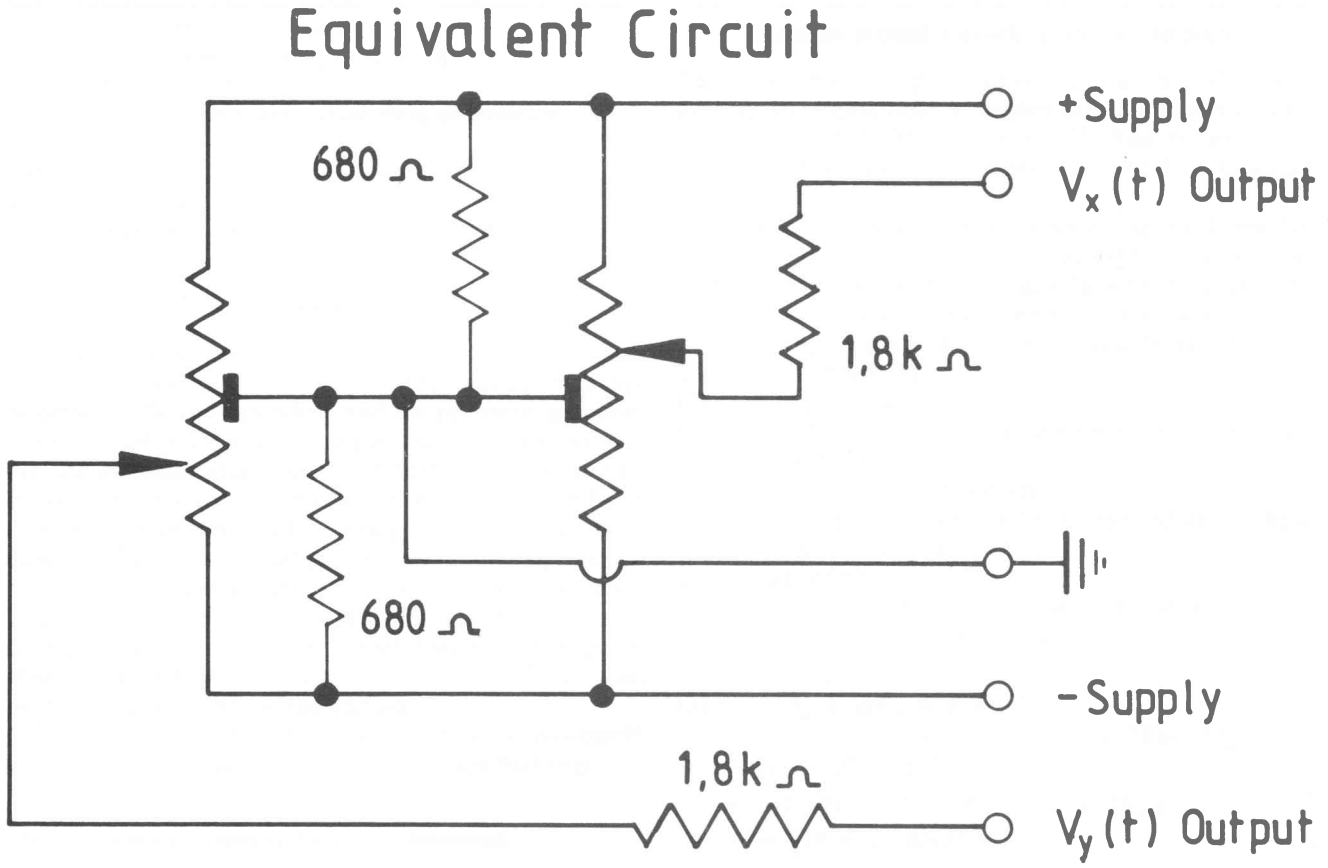

Typical specification	
Supply Voltage	4.75V to 15V
Current Drain*	15mA
Operating Frequency	20kHz (nom.)
Output Impedances	1.8kOhms (Signals) 0.34kOhms (centre tap)
Ripple	Deflection voltage/100
Noise	Nil
Centre Tap Voltage*	5V ± 10mV (relative to green centre tap)
Incremental Resolution	Infinite
Response Time	5mS (exponential)
Voltage Swing*	IV ± 10%
Life	10 Million Cycles
Sensor Wear Rate	Nil

*at 10V supply voltage

Appendix 3

Table 1

The following dimensions refer to Fig. 2.

Member/Item	Dimension	Comment
Probe	projected area 1 200 mm² (including rounded ends)	aluminium tube 20 mm dia.
D_D	278 mm	6 mm dia. silver steel (extending through probe)
Length of rod D_D	110 mm exposed to wind	
B-CM	37 mm	
B-D	85 mm	
R	105 mm	aluminium frying pan, cut to suit. (1.2 mm thickness)
Damping Vanes	25 000 mm²	0,7 mm thickness
Shaft assembly including skirting cage around electronics	978 g	includes transmitting coil
J moment of inertia (Shaft assembly	0,018 kg-m² (Fluid removed)	Determined experimentally for $\theta < 5°$
SAE-30 motor	888 kg/m³ 20 °C 91,9 centistokes	Courtesy Shell Refinery Dbn.
Power paraffin	814 kg/m³ 20 °C 1,8 centistokes	Courtesy Shell Refinery Dbn.
Liquid paraffin	850 kg/m³ 20 °C visc. >> 1,8 cS	
Reservoir	standard Shell oil 201 drum, 370 × 285 mm	
Shear plate	4 mm thick 442 mm dia. 15° chamfer	aluminium
Bouyant force on submerged pan and vanes.	1,18 N × S.G., (Variable f(θ))	acting 18 mm below D, determined exp.